MetOcean Solutions

Nelson Regional Sewerage Business Unit

NRSBU Overflow following upgrade model

Report prepared for
NRSBU

Specialists in Oceanography

MetOcean Solutions Ltd: P0356-01

September 2017

Report status

Version	Date	Status	Approved by
RevA	28/09/2017	Draft for internal review	Beamsley
RevB	29/09/2017	Draft for internal review	Berthot
RevC	29/09/2017	Draft for client review	Beamsley

It is the responsibility of the reader to verify the currency of the version number of this report.

TABLE OF CONTENTS

LIST OF FIGURES

LIST OF TABLES

1. INTRODUCTION

The Nelson Regional Sewerage Business Unit (NRSBU) is seeking a Resource Consent to land, Coastal Marine Area (Waimea Inlet, Figure 1.1) and Air from accidental wastewater overflow from four pump stations located on the edge of Waimea Inlet (Airport, Songer, Saxton and Wakatu, Figure 1.1), and from the pipework or pipeline fittings that make up the infrastructure of the Nelson Regional Sewerage Business Unit network. In order to understand the dilution characteristics of potential accidental wastewater discharges from the four pump stations NRSBU has commissioned MetOcean Solutions to undertake a numerical investigation into the expected discharge characteristics under a range of conservative scenarios.

The discharges from the pump stations arise as a result of emergency overflows and/or accidental discharges from pipeline failures or leakage. Specifically,

- Overflow discharges which occur as a result of excess flow (for example due to a heavy rain event)
- Overflow discharges due to pump station failure (for example due to equipment failure)
- Accidental discharges, which occur principally due to the accidental rupture or leakage from pipework or pipeline fittings
- Associated discharges of odour

The discharges are of largely untreated (screened) municipal sewage. Overflow discharges occur intermittently at the Nelson Airport, Saxton Street, Songer Street and Whakatu pump stations. Discharges occur either directly to the coastal marine area (Nelson Airport and Songer Street pump stations) or to land and then the coastal marine area (Whakatu and Saxton Street pump stations). The outlet of the discharge locations are shown in Figure 1.2

In order to understand the associated dilution rates and discharge characteristics within the Waimea Inlet, a range of numerical model simulations designed to bracket the likely dilution and discharge characteristics are needed. This modelling is intended to extend upon the calibrated and validated hydrodynamic model of the Waimea Inlet and environs maintained by MetOcean.

This report is structured as follows. An introduction to the study background and rational is provided in Section 1, while methods applied, including numerical model definitions are provided in Section 2. Results are presented in Section 3 and a concise summary is provided in Section 4. References cited are given in Section 5.

Figure 1.1 Waimea Inlet and pump discharge locations

Figure 1.2 Overflow pipe outlets from Waikatu, Saxton, Airport and Songer pump stations (from clockwise beginning top left)

2. METHODOLOGY

2.1. Modelling approach

The discharges from the pump stations arise as a result of emergency overflows and/or accidental discharges from pipeline failures or leakage. The outcome and timing of such releases is inherently non deterministic (i.e. unknown) and is governed, in part, by random variables such as currents, turbulences, wastewater network use, tidal stage, wind conditions and precipitation/fluvial discharges.

However, estuarine conditions under different forcing conditions can be assessed; thereby allowing the general geographical dispersion of the discharges to be determined. In the present study, a range of realistic simulations have been undertaken in order to bracket the expected dispersion and dilution characteristics of stormwater discharges from the Waikatu, Saxton, Airport and Songer pump stations in the unlikely event of an unexpected discharge.

2.2. Hydrodynamic model

2.2.1. Model description

The 2D baroclinic hydrodynamics of the Waimea Inlet were modelled using the open-source hydrodynamic model SCHISM[1][2]. The benefit of using open-source science models is the full transparency of the code and numerical schemes, and the ability for other researchers to replicate and enhance any previous modelling efforts for a given environment.

SCHISM is a prognostic finite-element unstructured-grid model designed to simulate 2D-3D baroclinic or 2D barotropic circulation. The barotropic mode equations employ a semi-implicit finite-element Eulerian-Lagrangian algorithm to solve the shallow-water equations, forced by relevant physical processes (atmospheric, oceanic and fluvial forcing). A detailed description of the SCHISM model formulation, governing equations and numerics, can be found in Zhang and Baptista (2008).

The SCHISM model is physically realistic, in that well-understood laws of motion and mass conservation are implemented. Therefore, water mass is generally conserved within the model, although it can be added or removed at open boundaries (e.g. through tidal motion at the ocean boundaries) and water is redistributed by incorporating aspects of the real-world systems (e.g. bathymetric information, forcing by tides and wind). The model transports water and other constituents (e.g. salt, temperature, turbulence) through the use of triangular volumes (connected 3-D polyhedrons).

The finite-element triangular grid structure used by SCHISM has resolution and scale benefits over other regular or curvilinear based hydrodynamic models. SCHISM is computationally efficient in the way it resolves the shape and complex bathymetry associated with estuaries, and the governing equations are similar to other open-source models such as Delft3D and ROMS. SCHISM has been used extensively within the scientific community[3],[4] where it forms the backbone of

[1] http://ccrm.vims.edu/schism/
[2] http://www.ccrm.vims.edu/w/index.php/Main_Page#SCHISM_WIKI
[3] http://www.stccmop.org/knowledge_transfer/software/selfe/publications
[4] http://ccrm.vims.edu/schism/schism_pubs.html

operational systems used to nowcast and forecast estuarine water levels, storm surges, velocities, water temperature and salinity[5].

2.2.2. Model domain and bathymetry

Bathymetry was sourced from a combination of LIDAR data supplied by NCC and ENC navigational charts. Because of the relatively poor bathymetric coverage in some of the channels within the Waimea Inlet, some depth contours were manually added based on aerial images and the relatively coarse ENC data. These channel depths were additionally adjusted as part of the model calibration and validation process.

The model resolution was optimised to ensure replication of the salient hydrodynamic processes. The resolution ranged from 120 m at the offshore boundary to 15 m in shallow water and near the coast, with grid refinement in the main intertidal channels and within the open rivers boundary, streams and creeks. The triangular elements of the model domain are shown in Figure 2.1 and associated bathymetry is presented in Figure 2.2.

[5] https://tidesandcurrents.noaa.gov/ofs/creofs/creofs_info.html

Figure 2.1 Waimea Inlet model domain showing the Finite-Element triangular model mesh for the entire model domain (top) and in the vicinity of the pump stations discharge point (bottom)

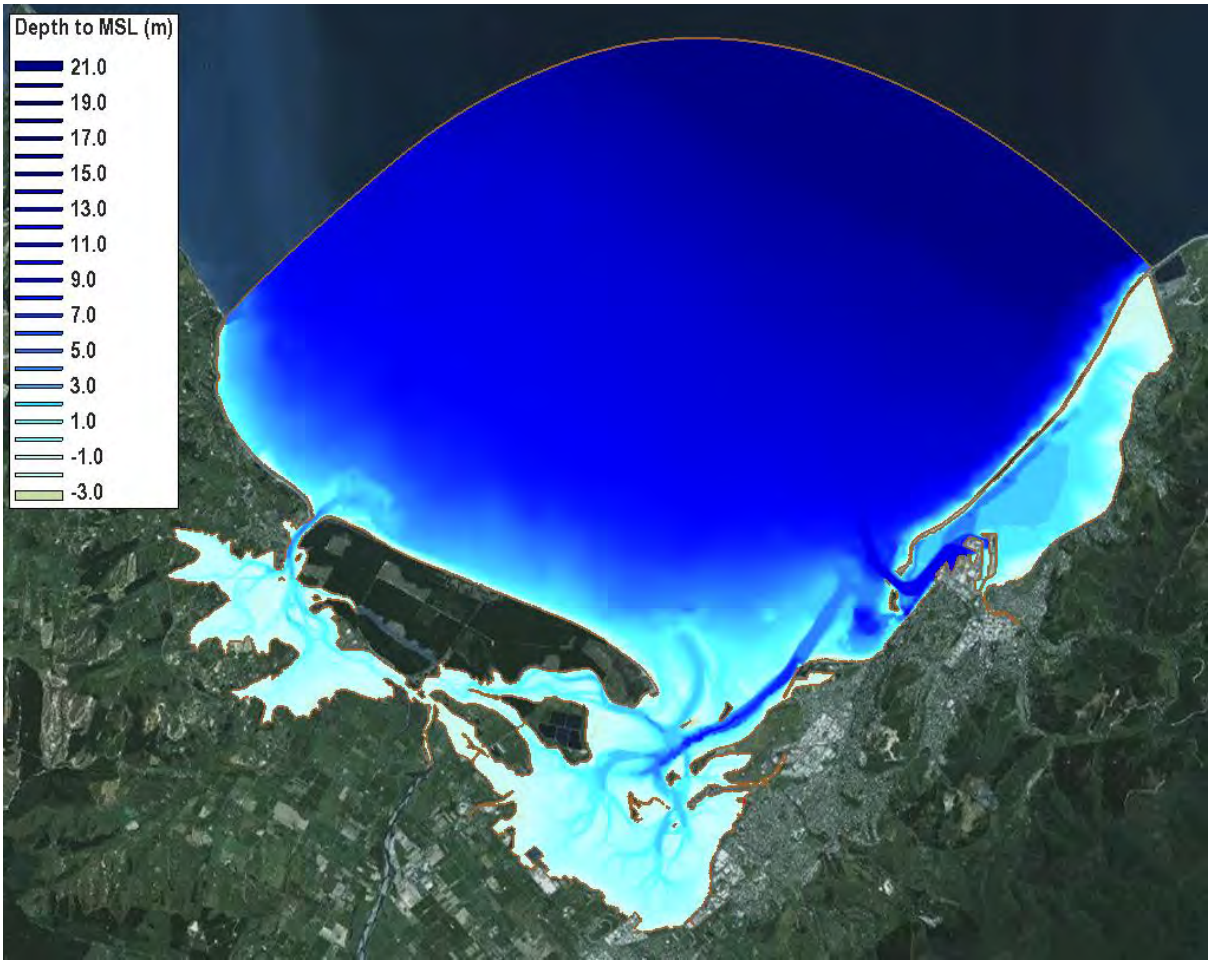

Figure 2.2 Waimea Inlet model domain showing the model bathymetry. Depths are given to Mean Sea Level (MSL)

2.2.3. Vertical mixing / turbulence closure

Vertical mixing was modelled using a constant diffusivity for momentum and transport of 1e-06. These values were adjusted as part of the model validation and calibration process.

Frictional stress at the seabed was calculated using a manning formulation using a coefficient of 0.02.

2.2.4. Modelled scenarios

A range of scenarios have been modelled in order to bracket the expected dispersion and dilution characteristics of stormwater discharges from the pump stations in the unlikely event of an unexpected discharge. Each of the simulations is unique in terms of the initial tidal state, forcing conditions and pump discharge rates, and chosen based on client guidance. The conditions simulated are provided in Table 2.1 and Figure 2.3, while Table 2.2 and Table 2.3 detail the associated fluvial and stormwater discharges respectively. Open boundary locations for each of the fluvial and stormwater discharges are shown in Figure 2.4.

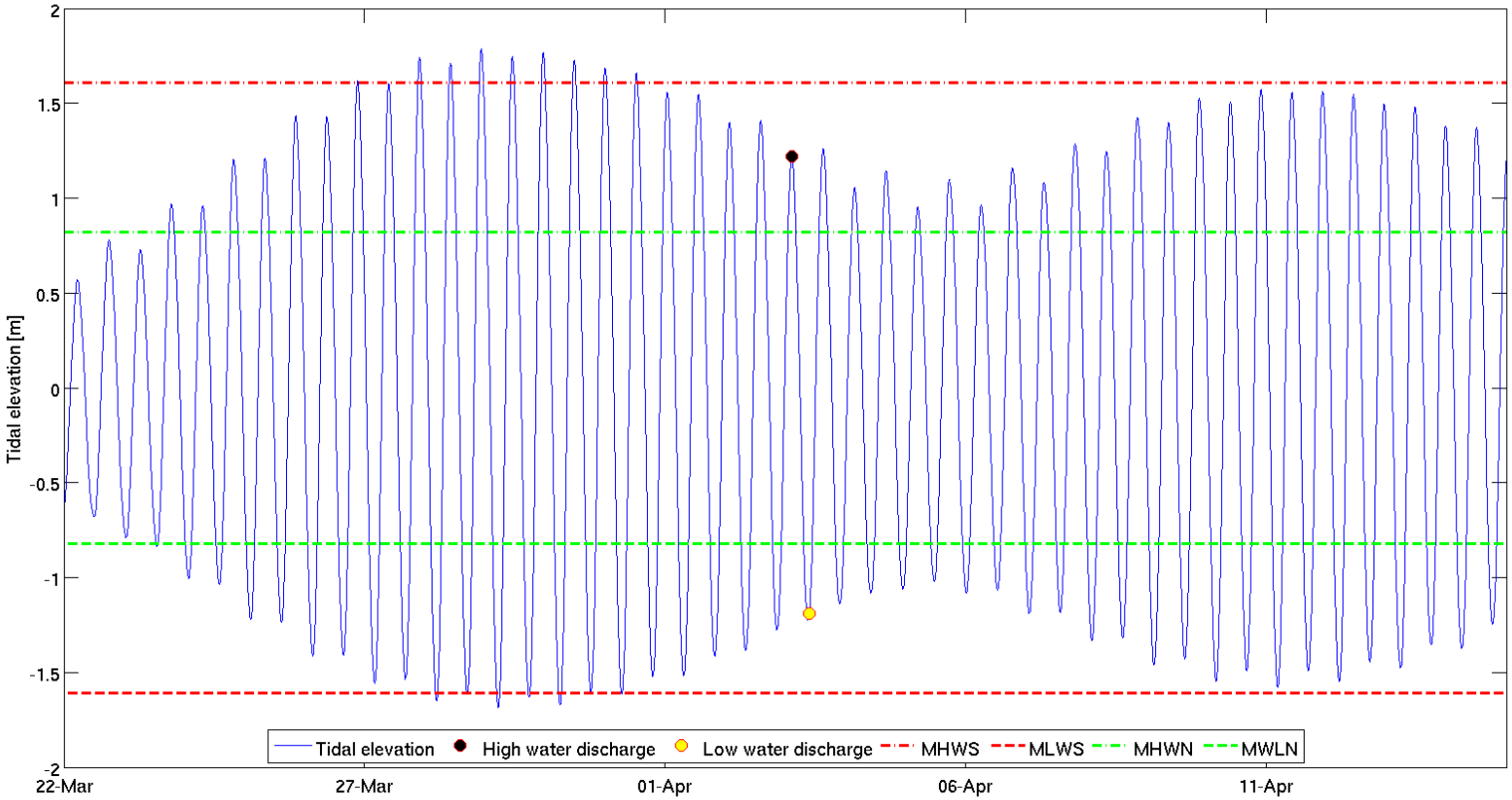

Figure 2.3 Time series of tidal elevation inside the Waimea Inlet showing the time of the high water discharge (black dot) and low water discharge (yellow dot) in relation to mean high water spring (MHWS), mean low water spring (MLWS), mean high water neap (MHWN) and mean low water neap (MLWN)

Table 2.1 Model scenarios

Weather	Tide at start of release	Wind velocity	Stormwater flow	River flow condition	Duration of stormwater discharge
Wet (high river flows)	MHW	22.5 degrees – 9 km.hr^{-1}	Peak flow m^3.hr^{-1}	90th percent discharge rate	4 hours
		135 degrees - 8.5 km.hr^{-1}	Peak flow m^3.hr^{-1}	90th percent discharge rate	4 hours
		Zero wind	Dry flow m^3.hr^{-1}	90th percent discharge rate	4 hours
	MLW	22.5 degrees – 9 km.hr^{-1}	Peak flow m^3.hr^{-1}	90th percent discharge rate	4 hours
		135 degrees - 8.5 km.hr^{-1}	Peak flow m^3.hr^{-1}	90th percent discharge rate	4 hours
		Zero wind	Dry flow m^3.hr^{-1}	90th percent discharge rate	4 hours
Dry (Low river flows)	MHW	22.5 degrees – 9 km.hr^{-1}	Peak flow m^3.hr^{-1}	15th percent discharge rate	4 hours
		135 degrees - 8.5 km.hr^{-1}	Peak flow m^3.hr^{-1}	15th percent discharge rate	4 hours
		Zero wind	Dry flow m^3.hr^{-1}	15th percent discharge rate	4 hours
	MLW	22.5 degrees – 9 km.hr^{-1}	Peak flow m^3.hr^{-1}	15th percent discharge rate	4 hours
		135 degrees - 8.5 km.hr^{-1}	Peak flow m^3.hr^{-1}	15th percent discharge rate	4 hours
		Zero wind	Dry flow m^3.hr^{-1}	15th percent discharge rate	4 hours

Table 2.2 Model open fluvial boundary conditions for wet and dry conditions (i.e. 90th and 15th percentile respectively)

Open river boundaries	90th percentile ($m^3.s^{-1}$)	15th percentile ($m^3.s^{-1}$)
Waimea River	38.8000	2.4000
Neimann Creek	0.1000	0.0480
Jenkins Creek	0.1103	0.0048
Maitai River	4.2870	0.4540
Poorman @ Seaview	0.1003	0.0144
Orphanage @ Ngawhatu	0.1569	0.0076
Jenkins @ Pascoe St	0.1103	0.0048
Saxton @ below confluence	0.1038	0.0005

Table 2.3 Peak and dry discharge rates for each of the pump stations

Pump Station	Peak discharge rate ($m^3.s^{-1}$)	Dry flow discharge rate ($m^3.s^{-1}$)	Duration
Airport	0.1400	0.0353	4 hours
Songer	0.0847	0.0144	4 hours
Saxton	0.4325	0.0900	4 hours
Wakatu	0.0119	0.0014	4 hours

Figure 2.4 Open fluvial (white text) and pump station (blue text) boundaries within the Waimea Inlet and Nelson Harbour.

2.2.1. Offshore tidal forcing

The widely used tidal constituents sourced to force regional and coastal domains in hydrodynamic models - the Oregon State University Tidal Inverse Solution (OTIS, Egbert and Erofeeva, 2002) – was rather coarse for direct use in New Zealand coastal domains. Therefore, tidal constituents from the harmonic analysis of a long term 2D Princeton Ocean Model (POM, Mellor, 1998) tidal simulation with 5 km horizontal resolution were used to derive tidal boundaries for the Waimea Inlet SCHISM model.

The NZ-POM domain was forced at the open boundaries by tidal elevation and current harmonic constituents derived from the OTIS Pacific Ocean solution[6]. The Waimea Inlet SCHISM domain was forced at the open boundary by elevation and current constituents derived from the POM 2D simulation.

2.2.1. Model calibration and validation

The physics of the Waimea Inlet SCHISM hydrodynamic model has been calibrated and validated as part of the Bell Island discharge modelling study, and a complete description of the process can be found in MetOcean Solutions Ltd (2017).

2.3. Dilution and concentrations with Eulerian tracers

Eulerian tracer is a concentration field that obeys a classical advection-diffusion equation driven with currents of the hydrodynamic model (Meier and Höglund, 2013). Deleersnijder *et al.* (2001) presented a detailed description of Eulerian tracer theory applied to the age distribution of seawater. Sources, sinks and initial and boundary conditions are specified for the tracer under consideration. For this study, within the modelling framework the Eulerian tracers are tracked and relative dilution rates are determined within a spatial context by considering the initial concentration or relative dilution at the discharge point. A key output of this modelling is the supply of time-varying dilution fields.

According to Zhang *et al.* (2010), the “mean tracer age” is calculated from the mean of the spectrum, which is defined as “the mass-weighted, arithmetic average of the time elapsed since the tracer left the source region”. The “mean residence time” is defined as “the mass-weighted, arithmetic average of the time needed for the tracer to leave a domain of interest”.

The water age represents the mean age of the water in a grid cell of the numerical model used, and this value results from the mixing of water parcels of different ages within each cell (Andrejev et al., 2004), with associated dilution rates.

A detailed description of Eulerian tracer technique to obtain water age, residence time and associated dilution is presented in Zhang *et al.* (2010). These authors investigated the time scales associated with the spreading of the Hudson River source waters across the inner shelf of New York Bight. Differing from the common Lagrangian approach, which is characterised by the release of many tracers and extracting time-scale information from their differential transport, Eulerian tracer technique is computationally much cheaper (Zhang et al., 2010). However, it does not give full details with regards to the water parcel composition and age, as it gives average age inside each grid cell. Still it is a very useful technique for studying spatial patterns of circulation and mixing and the associated time scales

[6] http://volkov.oce.orst.edu/tides/PO.html

(Hall and Haine, 2002; Zhang et al., 2010), and is appropriate for this study given the relatively high model resolution of the receiving environment.

3. RESULTS

3.1. Model hydrodynamics

Examples of the mean current speed during peak ebb and flood tides are provided in Figure 3.1 and Figure 3.2 respectively, and illustrate that the strongest current speeds occur within the channels.

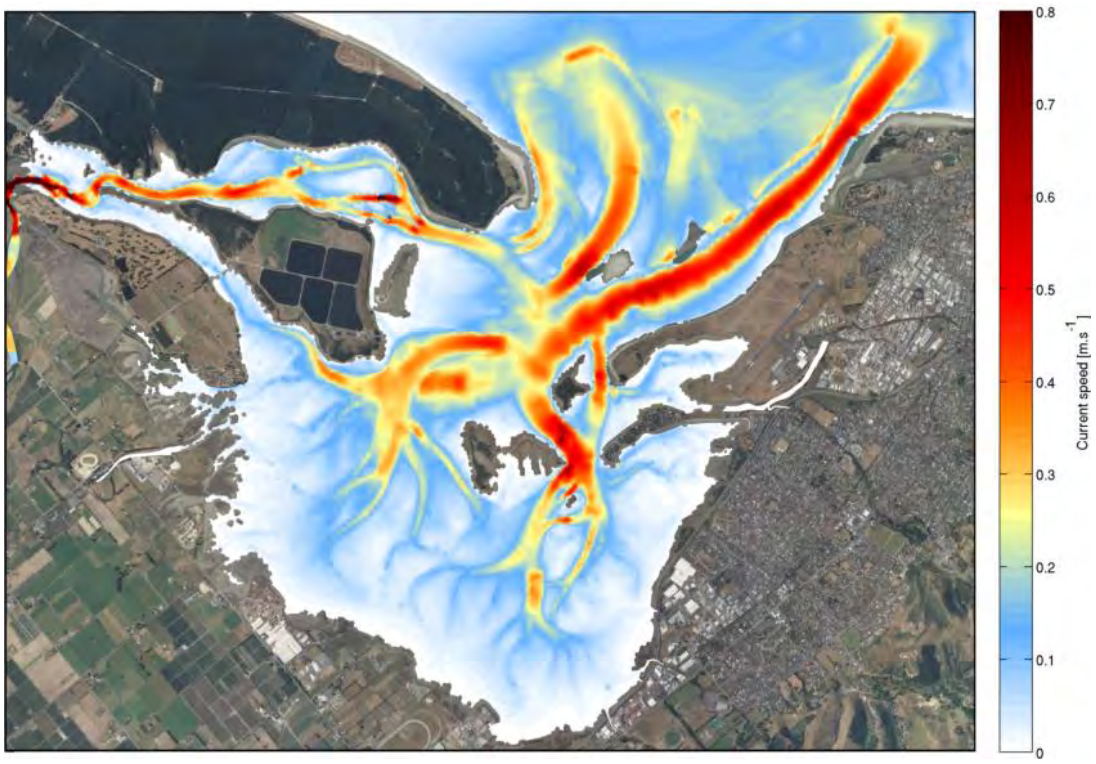

Figure 3.1 Mean current speed during peak flood tide inside the Waimea Inlet

Figure 3.2 Mean current speed during peak ebb tide inside the Waimea Inlet

3.2. Individual pump station discharge concentration.

3.2.1. Airport pump station

Model predicted dilution fields at 2, 4 and 6 hours after a 4-hour discharge from the Airport pump station discharge point at MHW and MLW with relatively low fluvial discharges (dry) are provided in Figure 3.3 and Figure 3.4 respectively. Dilution fields under relatively elevated fluvial discharges (wet) are provided in Figure 3.5 and Figure 3.6 for MHW and MLW respectively. Discharge scenarios are summarised in Table 2.1, while Table 2.2 and Table 2.3 provide details of the associated fluvial discharges for wet and dry conditions and the pump station discharge rates accordingly. The model domain has been established such that ponding of the discharge occurs at the discharge location consistent with the discharge point characteristics (Figure 1.2), so that while active discharging occurs only over a 4-hour period, results show waste-water moving away from the initial discharge location at the 6 hour mark also.

The spatial distribution of the discharged waste water at MHW initially increases expectedly due to the ebbing tide. The rate of increase in the spatial extent reduces as MLW is approached at approximately 6 hours after the initial release. As expected, both wind events modelled act to increase the dilution rate of the discharged waste water relative to the no-wind event. The two wind events simulated result in broadly similar spatial distributions in the dilution fields, presumably due to the relatively low wind speeds (i.e. < 5 knots, see Figure 3.3 and Figure 3.5).

The spatial distribution of the discharged waste water at MLW initially increase as the waste water disperses over the exposed intertidal flats and associated intertidal channels. At the 4 hour mark the flooding tide effectively confines the discharged waste water to the immediate vicinity of the discharge point, and the spatial extent of the dilution field decreases. At 6 hours after MLW the momentum of the discharged waste water overcomes the tidal forcing and the plume of waste water extends away from the discharge point. As expected, at 6 hour after the beginning of the discharge, both wind events modelled act to increase the dilution rate of the discharged waste water and the spatial coverage relative to the no-wind event. The two wind events simulated result in broadly similar spatial distributions in the dilution fields, presumably due to the relatively low wind speeds (i.e. < 5 knots, see Figure 3.4 and Figure 3.6). The spatial distribution at this time is consistent with the tidal stage approaching MHW and the intertidal areas being inundated.

For both the MHW and MLW discharges the expected dilution rates are broadly similar for both the ‘wet’ and ‘dry’ discharges due to the balance between the increased discharge rate from the pump stations and increased effective dilution due to increased fluvial discharges.

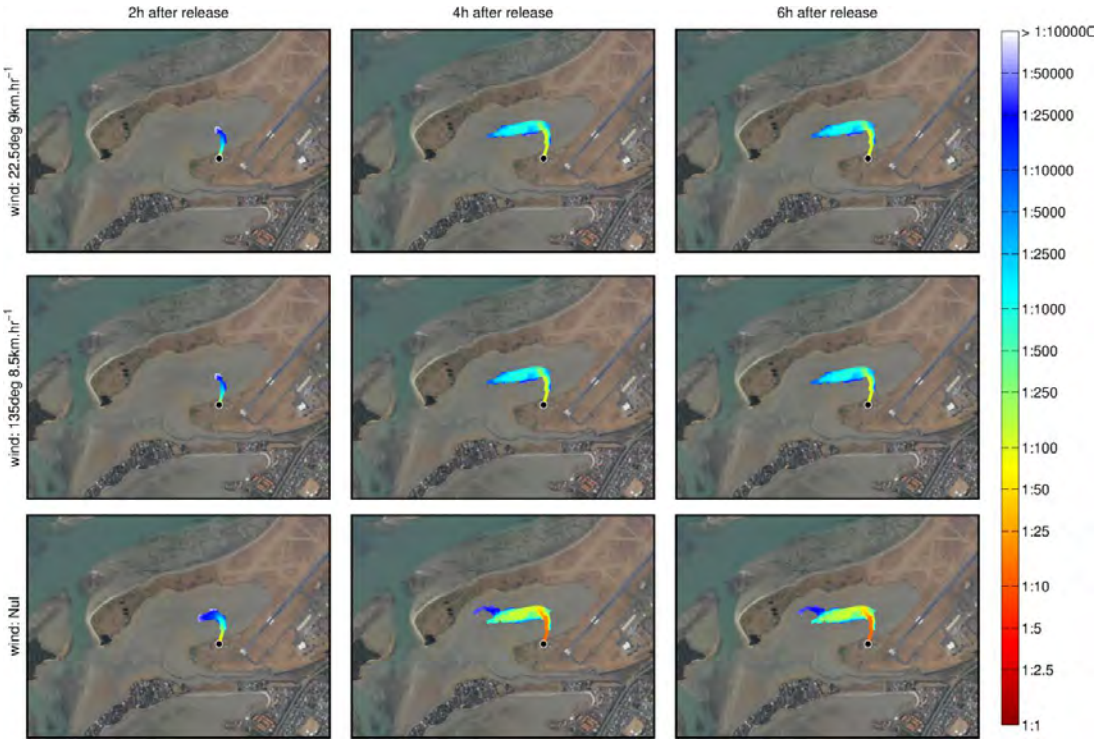

Figure 3.3 Dilution at airport pump station 2h (left column), 4h (middle column) and 6h (right column) after a release of effluent at MHW under a dry river period in 3 different wind conditions.

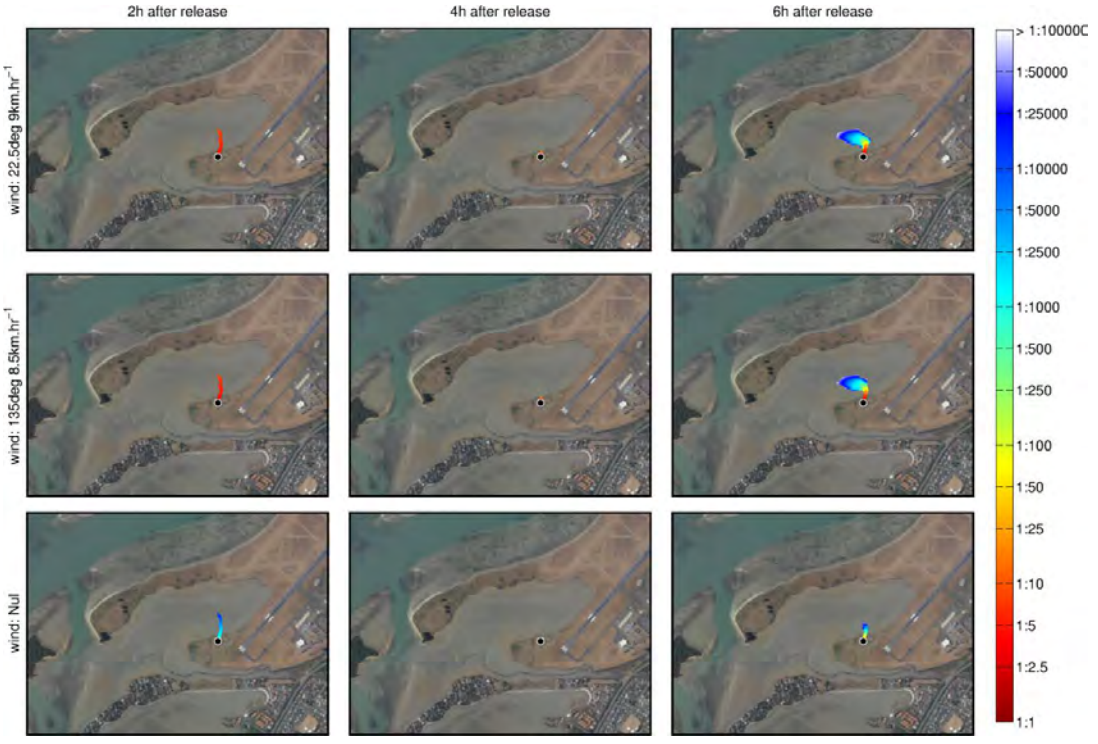

Figure 3.4 Dilution at airport pump station 2h (left column), 4h (middle column) and 6h (right column) after a release of effluent at MLW under a dry river period in 3 different wind conditions.

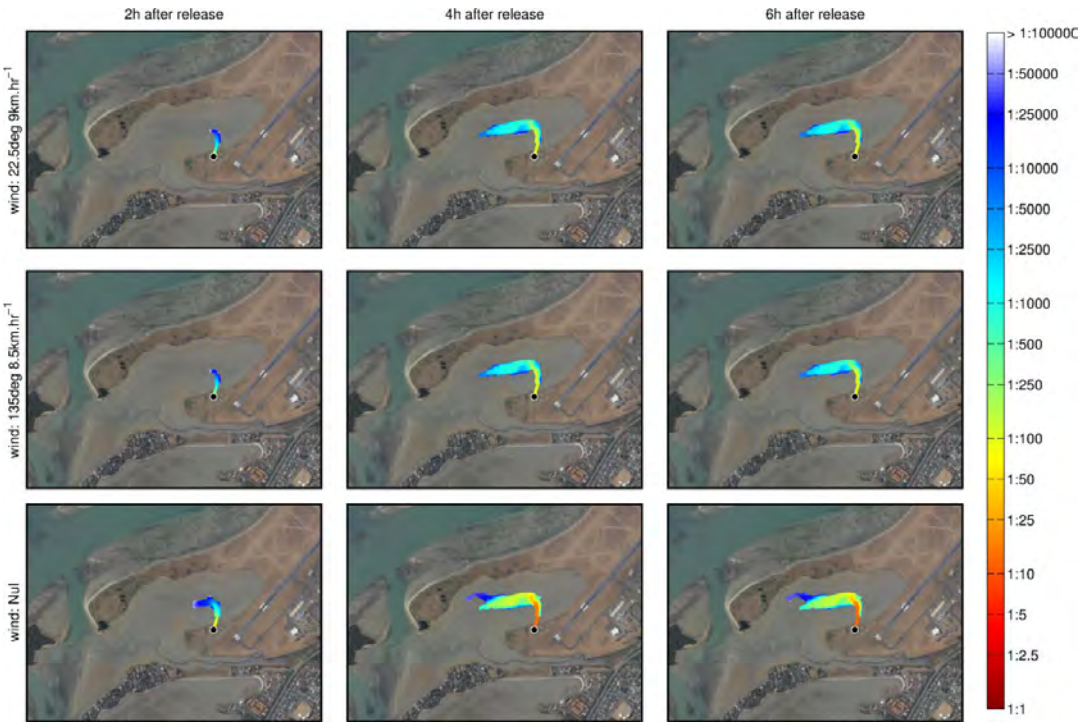

Figure 3.5 Dilution at airport pump station 2h (left column), 4h (middle column) and 6h (right column) after a release of effluent at MHW under a wet river period in 3 different wind conditions.

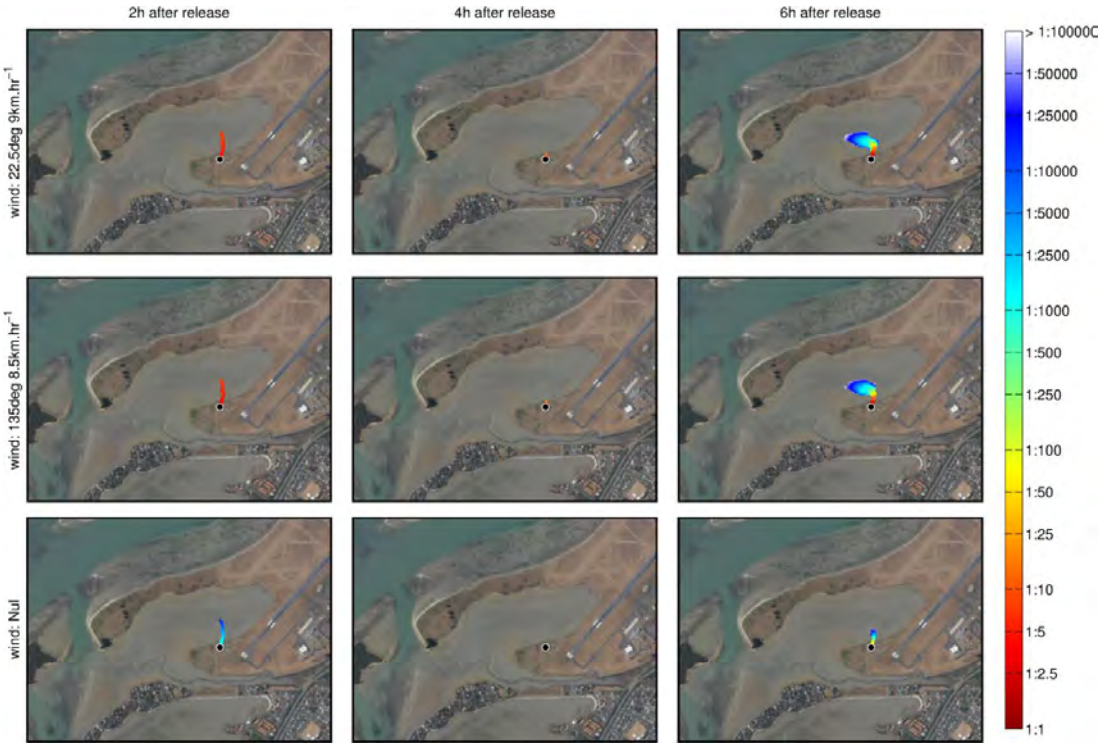

Figure 3.6 Dilution at airport pump station 2h (left column), 4h (middle column) and 6h (right column) after a release of effluent at MLW under a wet river period in 3 different wind conditions.

3.2.2. Songer pump station

Model predicted dilution fields at 2, 4 and 6 hours after a 4-hour discharge from the Songer pump station discharge point at MHW and MLW with relatively low fluvial discharges (dry) are provided in Figure 3.7 and Figure 3.8 respectively. Dilution fields under relatively elevated fluvial discharges (wet) are provided in Figure 3.9 and Figure 3.10 for MHW and MLW respectively. Discharge scenarios are summarised in Table 2.1, while Table 2.2 and Table 2.3 provide details of the associated fluvial discharges for wet and dry conditions and the pump station discharge rates accordingly. The model domain has been established such that ponding of the discharge occurs at the discharge location consistent with the discharge point characteristics (Figure 1.2), so that while active discharging occurs only over a 4-hour period, results show waste-water moving away from the initial discharge location at the 6 hour mark also.

The spatial distribution of the discharged waste water at MHW under wind events initially increases expectedly due to the ebbing tide and the inundation of the intertidal areas. The spatial extent reduces as MLW is approached at approximately 6 hours after the initial release. Both wind events modelled act to increase the dilution rate of the discharged waste water relative to the no-wind event, while the wind event from the SE (i.e. 135°T) increases the northerly excursion of the plume. Irrespective, the two wind events simulated result in broadly similar spatial distributions in the dilution fields, presumably due to the relatively low wind speeds (i.e. < 5 knots, see Figure 3.7 and Figure 3.9). In contrast, the discharge of wastewater under no-wind conditions from Songer pump station at MHW results in very limited plume extents due to the relatively shallow intertidal flats within the area and the ponding of the discharge.

The spatial distribution of the discharged waste water at MLW is very limited due to the relatively shallow intertidal flats within the area and the ponding of the discharge. At 6 hours after MLW the momentum of the discharged waste water overcomes the tidal forcing and the plume of waste water extends away from the discharge point. As expected, at 6 hour after the beginning of the discharge, both wind events modelled act to increase the dilution rate of the discharged waste water and the spatial coverage relative to the no-wind event. The two wind events simulated result in broadly similar spatial distributions in the dilution fields, presumably due to the relatively low wind speeds (i.e. < 5 knots, see Figure 3.8 and Figure 3.10). The spatial distribution at this time is consistent with the tidal stage approaching MHW and the intertidal areas and channels being inundated.

For both the MHW and MLW discharges the expected dilution rates are broadly similar for both the ‘wet’ and ‘dry’ discharges due to the balance between the increased discharge rate from the pump stations and increased effective dilution due to increased fluvial discharges.

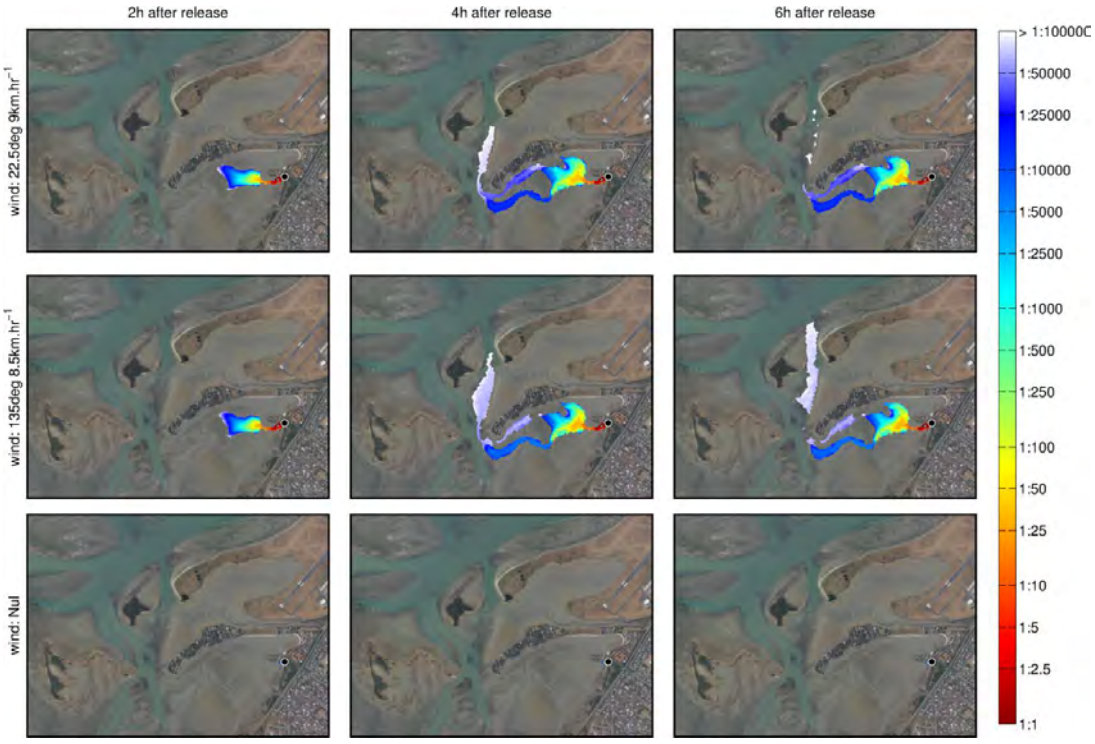

Figure 3.7 Dilution at Songer pump station 2h (left column), 4h (middle column) and 6h (right column) after a release of effluent at MHW under a dry river period in 3 different wind conditions.

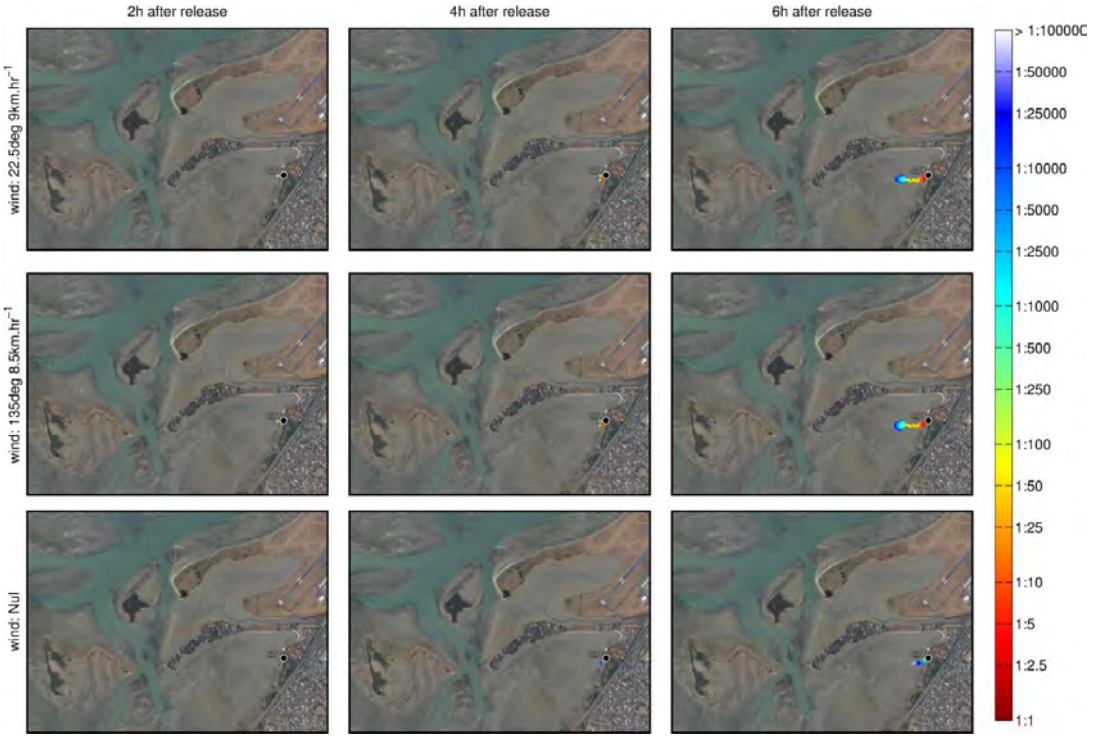

Figure 3.8 Dilution at Songer pump station 2h (left column), 4h (middle column) and 6h (right column) after a release of effluent at MLW under a dry river period in 3 different wind conditions.

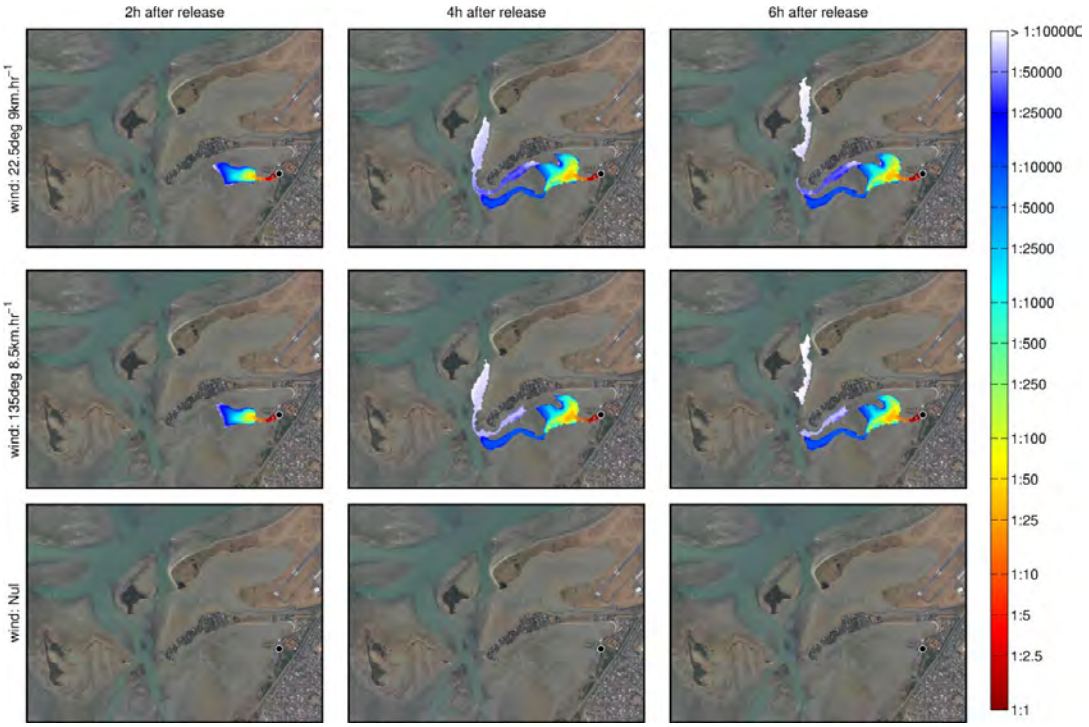

Figure 3.9 Dilution at Songer pump station 2h (left column), 4h (middle column) and 6h (right column) after a release of effluent at MHW under a wet river period in 3 different wind conditions.

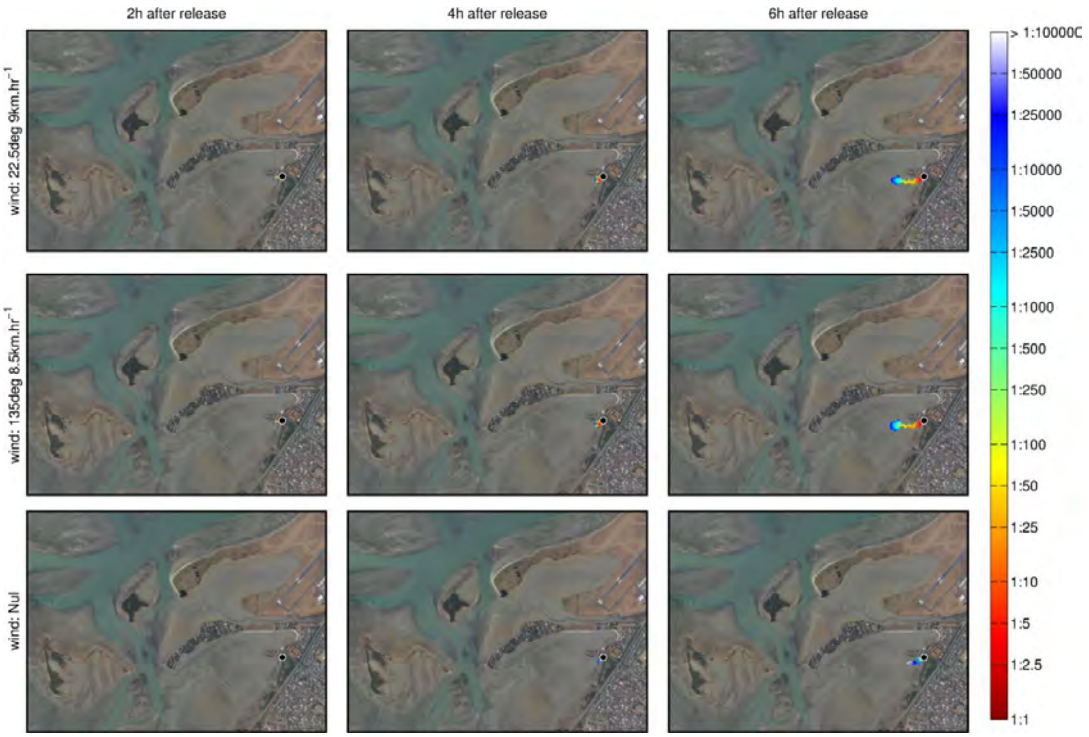

Figure 3.10 Dilution at Songer pump station 2h (left column), 4h (middle column) and 6h (right column) after a release of effluent at MLW under a wet river period in 3 different wind conditions.

3.2.3. Saxton pump station

Model predicted dilution fields at 2, 4 and 6 hours after a 4-hour discharge from the Saxton pump station discharge point at MHW and MLW with relatively low fluvial discharges (dry) are provided in Figure 3.11 and Figure 3.12 respectively. Dilution fields under relatively elevated fluvial discharges (wet) are provided in Figure 3.13 and Figure 3.14 for MHW and MLW respectively. Discharge scenarios are summarised in Table 2.1, while Table 2.2 and Table 2.3 provide details of the associated fluvial discharges for wet and dry conditions and the pump station discharge rates accordingly. The model domain has been established such that ponding of the discharge occurs at the discharge location consistent with the discharge point characteristics (Figure 1.2), so that while active discharging occurs only over a 4-hour period, results show waste-water moving away from the initial discharge location at the 6 hour mark also.

The spatial distribution of the discharged waste water at MHW increases expectedly due to the ebbing tide, and continues through the 6-hour period plotted due to the plume advecting to relatively deep water. As expected, both wind events modelled act to increase the dilution rate of the discharged waste water relative to the no-wind event. The two wind events simulated result in broadly similar spatial distributions in the dilution fields, presumably due to the relatively low wind speeds (i.e. < 5 knots, see Figure 3.11 and Figure 3.13).

The initial spatial distribution of the discharged waste water at MLW increase as the waste water disperses over the exposed intertidal flats and associated intertidal channels. At the 4 and 6 hour mark after the beginning of the discharge the dilution plume is relatively diffuse for both wind events modelled, with similar spatial extents, presumably due to the relatively low wind speeds (i.e. < 5 knots, see Figure 3.12 and Figure 3.14). In contrast, the plume associated with the no-wind event is confined to the vicinity of the discharge point due to the momentum balance between the flooding tide and the discharge rate.

For both the MHW and MLW discharges the expected dilution rates are broadly similar for both the ‘wet’ and ‘dry’ discharges due to the balance between the increased discharge rate from the pump stations and increased effective dilution due to increased fluvial discharges.

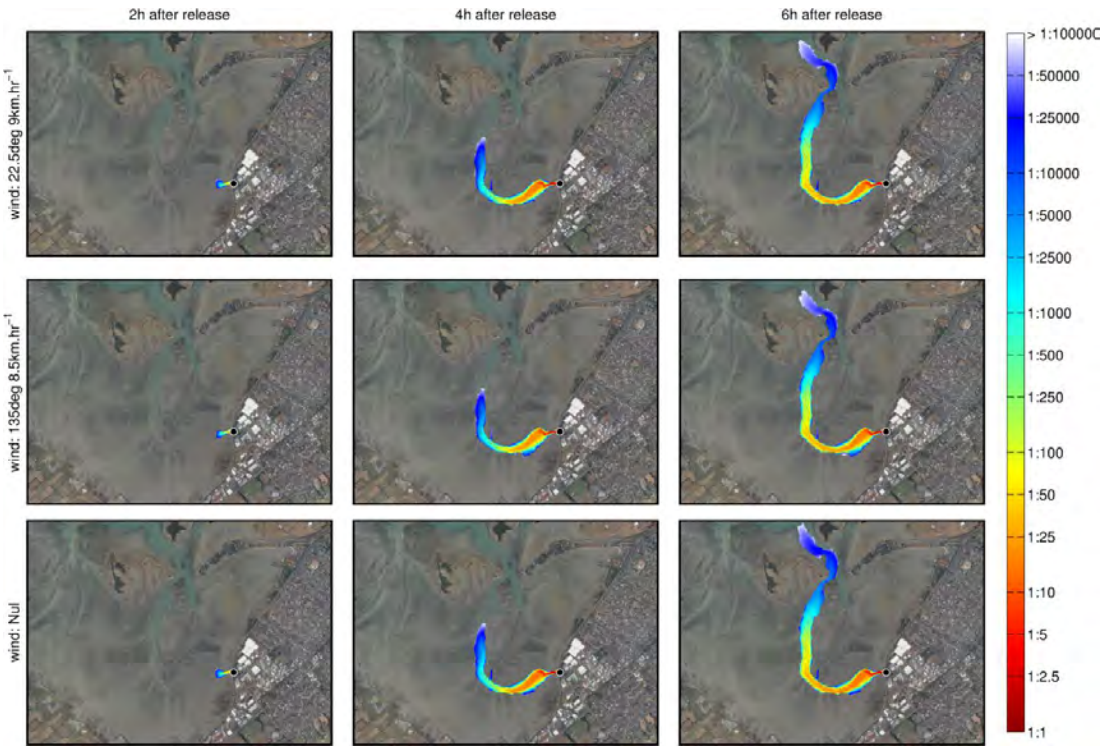

Figure 3.11 Dilution at Saxton pump station 2h (left column), 4h (middle column) and 6h (right column) after a release of effluent at MHW under a dry river period in 3 different wind conditions.

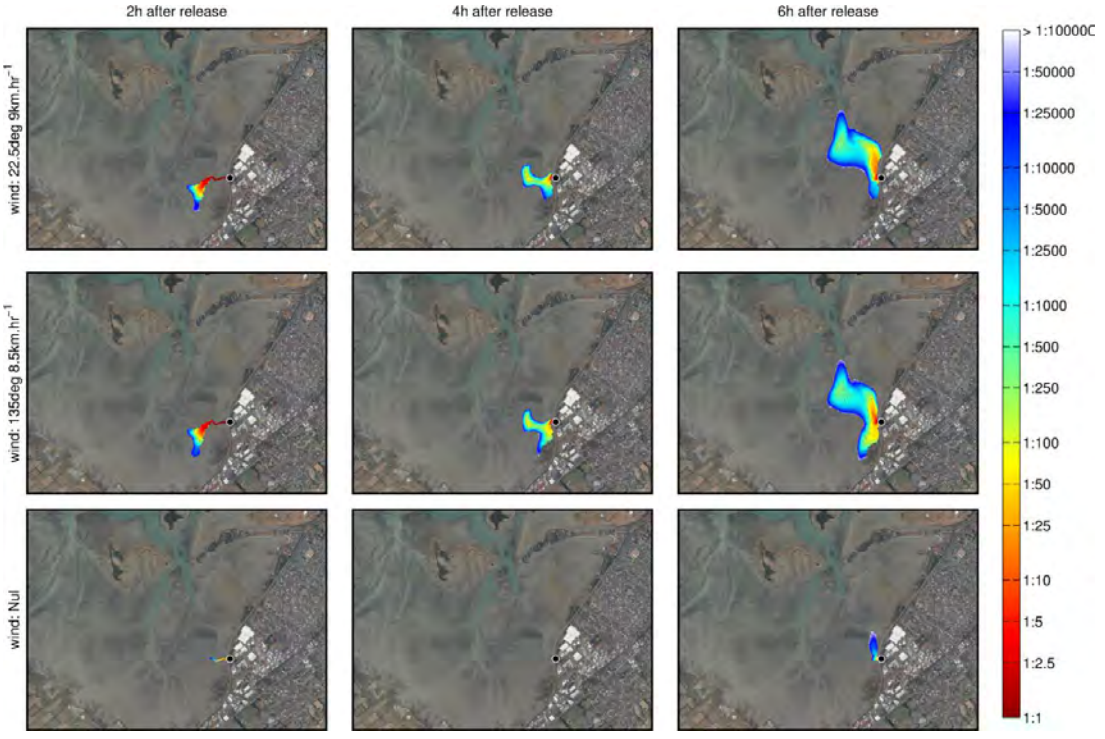

Figure 3.12 Dilution at Saxton pump station 2h (left column), 4h (middle column) and 6h (right column) after a release of effluent at MLW under a dry river period in 3 different wind conditions

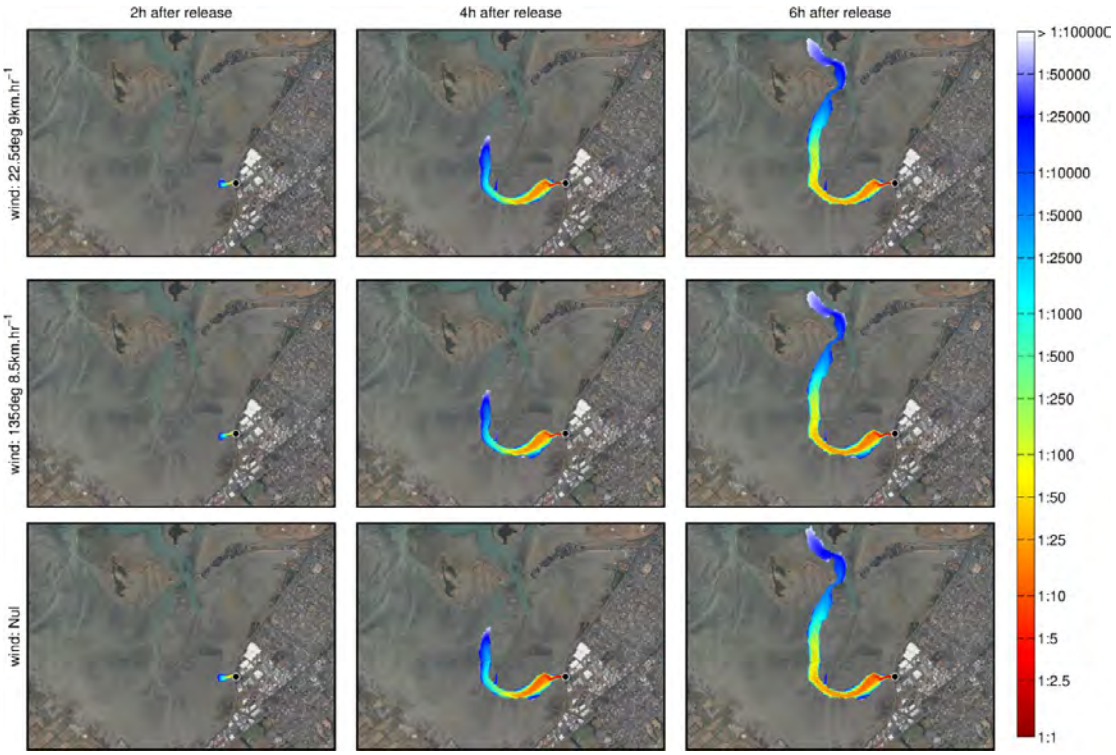

Figure 3.13 Dilution at Saxton pump station 2h (left column), 4h (middle column) and 6h (right column) after a release of effluent at MHW under a wet river period in 3 different wind conditions

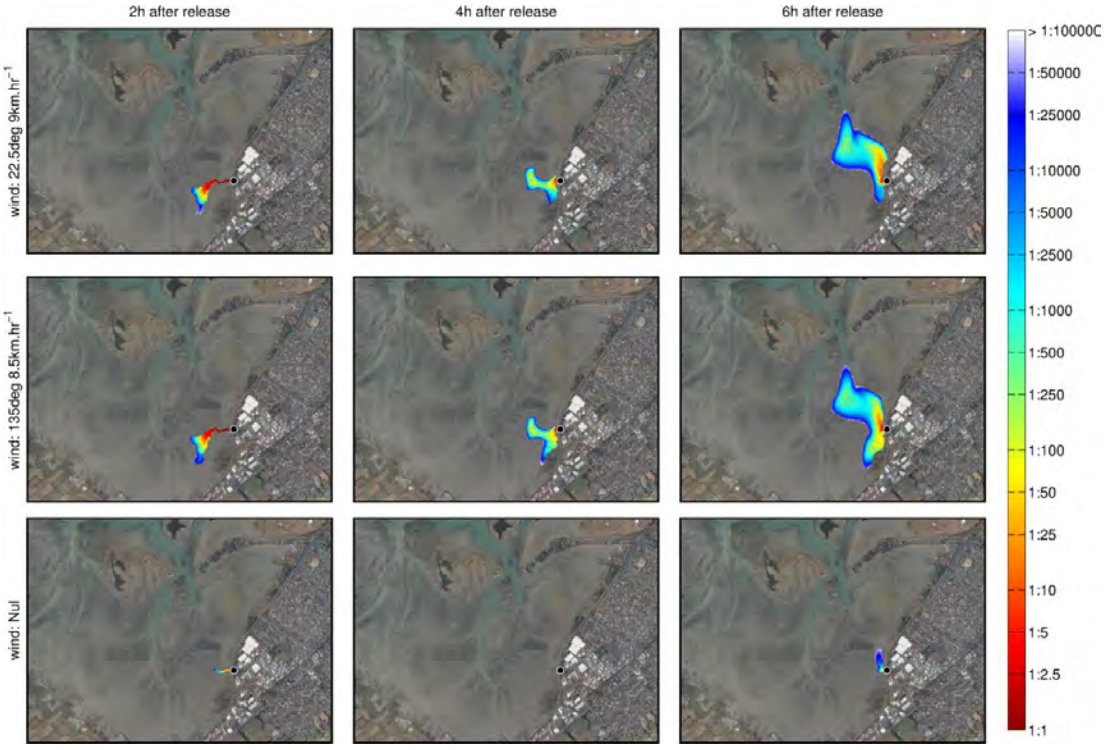

Figure 3.14 Dilution at Saxton pump station 2h (left column), 4h (middle column) and 6h (right column) after a release of effluent at MLW under a wet river period in 3 different wind conditions

3.2.4. Wakatu pump station

Model predicted dilution fields at 2, 4 and 6 hours after a 4 hour discharge from the Wakatu pump station discharge point at MHW and MLW with relatively low fluvial discharges (dry) are provided in Figure 3.15 and Figure 3.16 respectively. Dilution fields under relatively elevated fluvial discharges (wet) are provided in Figure 3.17 and Figure 3.18 for MHW and MLW respectively. Discharge scenarios are summarised in Table 2.1, while Table 2.2 and Table 2.3 provide details of the associated fluvial discharges for wet and dry conditions and the pump station discharge rates accordingly. The model domain has been established such that ponding of the discharge occurs at the discharge location consistent with the discharge point characteristics (Figure 1.2), so that while active discharging occurs only over a 4-hour period, results show waste-water moving away from the initial discharge location at the 6 hour mark also.

The spatial distribution of the discharged waste water at MHW under wind events initially increases expectedly due to the ebbing tide and the inundation of the intertidal areas. The spatial extent at 4 and 6 hours post the start of the discharging process is similar, consistent with the discharge of waste water over intertidal flats and channels. Both wind events modelled act to increase the dilution rate of the discharged waste water relative to the no-wind event. The two wind events simulated result in broadly similar spatial distributions in the dilution fields, presumably due to the relatively low wind speeds (i.e. < 5 knots, see Figure 3.7 and Figure 3.9). In contrast, the discharge of wastewater under no-wind conditions from the Wakatu pump station at MHW results in very limited plume extents due to the relatively shallow intertidal flats within the area and the ponding of the discharge.

The spatial distribution of the discharged waste water at MLW is very limited due to the relatively shallow intertidal flats within the area and the ponding of the discharge. At 6 hours after MLW the momentum of the discharged waste water beings to overcome the tidal forcing and the plume of waste water extends slightly further away from the discharge point. As expected, at 6 hour after the beginning of the discharge, both wind events modelled act to increase the dilution rate of the discharged waste water and the spatial coverage relative to the no-wind event. The two wind events simulated result in broadly similar spatial distributions in the dilution fields, presumably due to the relatively low wind speeds (i.e. < 5 knots, see Figure 3.8 and Figure 3.10).

For both the MHW and MLW discharges the expected dilution rates are broadly similar for both the ‘wet’ and ‘dry’ discharges due to the balance between the increased discharge rate from the pump stations and increased effective dilution due to increased fluvial discharges.

Figure 3.15 Dilution at Wakatu pump station 2h (left column), 4h (middle column) and 6h (right column) after a release of effluent at MHW under a dry river period in 3 different wind conditions

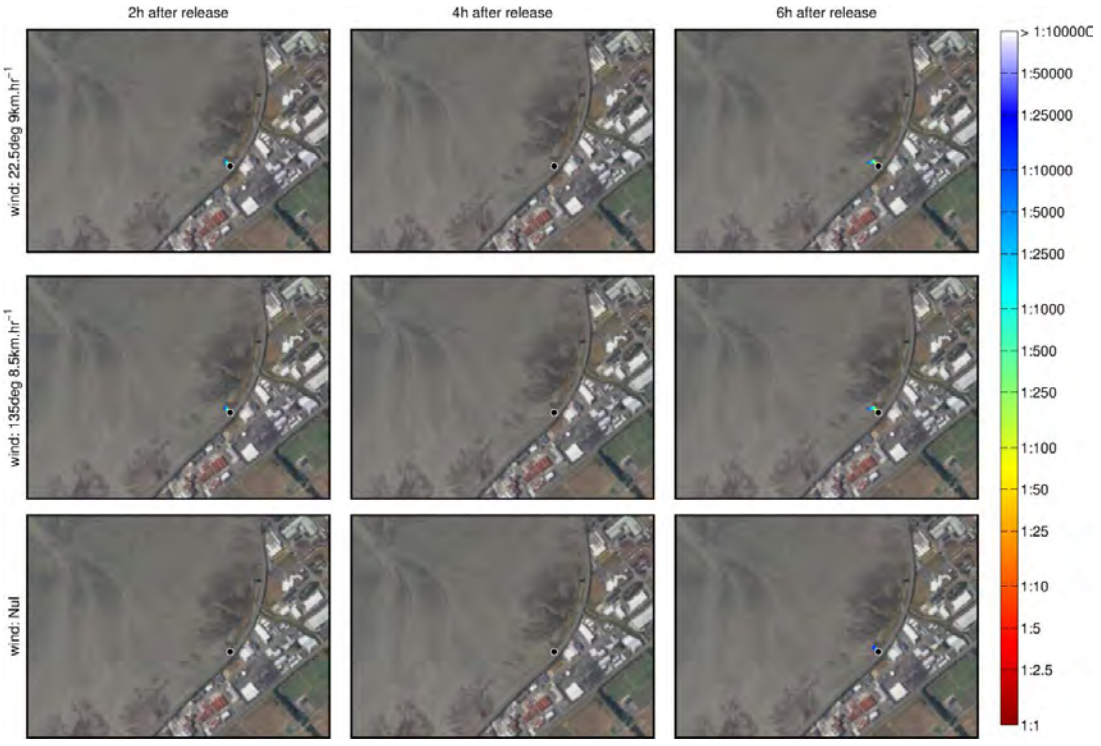

Figure 3.16 Dilution at Wakatu pump station 2h (left column), 4h (middle column) and 6h (right column) after a release of effluent at MLW under a dry river period in 3 different wind conditions

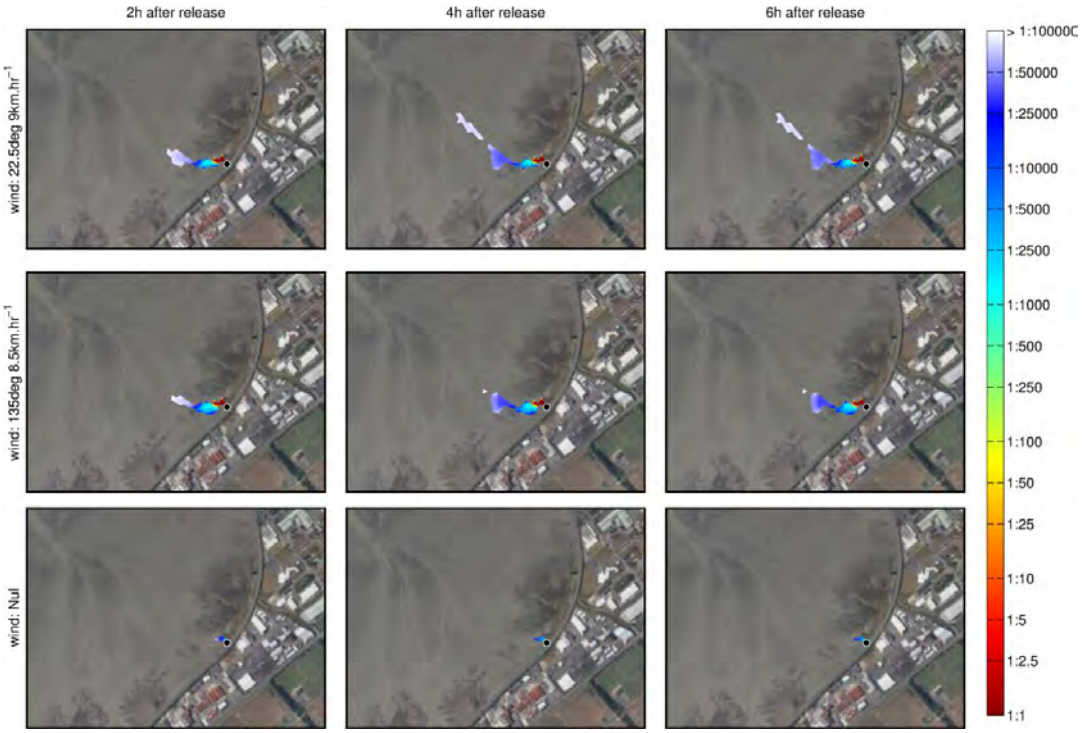

Figure 3.17 Dilution at Wakatu pump station 2h (left column), 4h (middle column) and 6h (right column) after a release of effluent at MHW under a wet river period in 3 different wind conditions

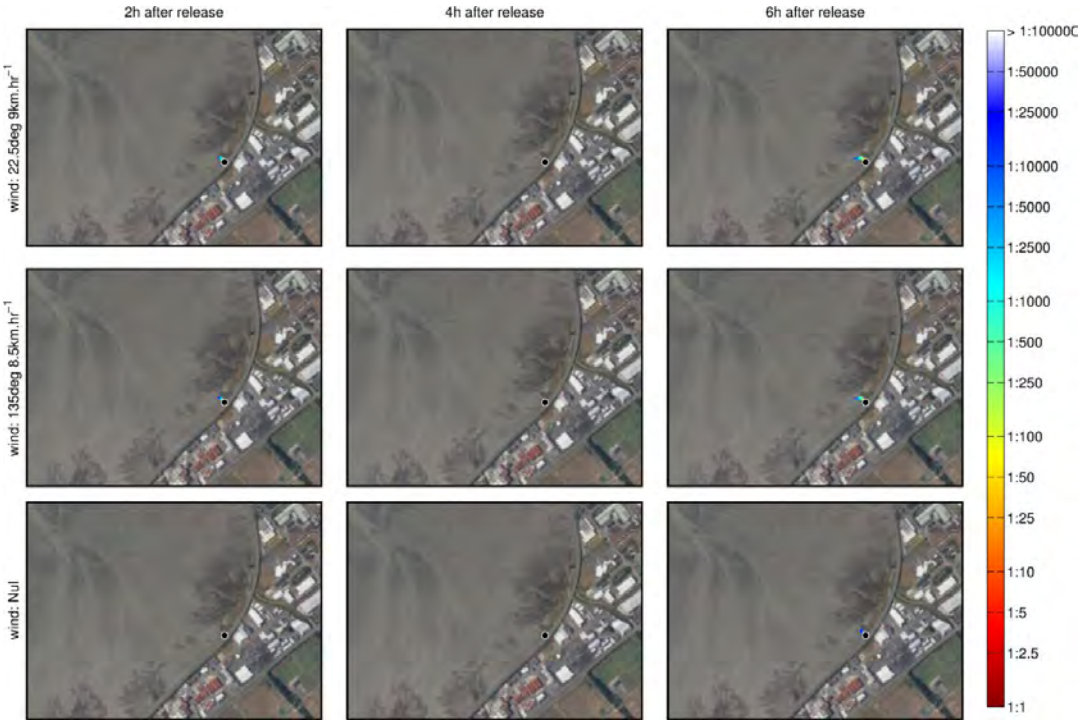

Figure 3.18 Dilution at Wakatu pump station 2h (left column), 4h (middle column) and 6h (right column) after a release of effluent at MLW under a wet river period in 3 different wind conditions

4. SUMMARY

Emergency overflow discharges from Airport, Songer, Saxton and Wakatu pump stations (Figure 1.1) have been modelled using a calibrated and validated hydrodynamic model of the Waimea Inlet. A range of discharge events have been modelled in order to bracket potential discharge characteristics by accounting for different discharge rates from the pump stations and considering 'wet' and 'dry' fluvial discharges from 8 different river/stream/creeks that discharge into the Waimea Inlet (Table 2.2). In addition, different wind forcing events have been considered. The model domain has been established such that ponding of the discharge occurs at the discharge location consistent with the discharge point characteristics (Figure 1.2), so that while active discharging only occurs over a 4-hour period, results show waste-water moving away from the initial discharge location at the 6 hour mark also.

Because of the intertidal nature of the discharge points (Figure 1.1, Figure 1.2), the dispersion and dilution of the potential waste water discharges has been simulated using Eulerian Tracers.

Pump station discharge rates and fluvial discharge fluxes were supplied by council and agreed upon amongst the working team prior to simulating the discharges.

For all pump stations the MHW and MLW discharges the expected dilution rates are broadly similar for both the 'wet' and 'dry' discharges due to the balance between the increased discharge rate from the pump stations and increased effective dilution due to increased fluvial discharges into Waimea Inlet.

For all pump stations the effect of the two wind conditions simulated (see Table 2.1) result in similar dispersion and dilution outcomes, with both the dispersion and dilution increased relative to the no-wind simulation.

For all pump stations under the spatial distribution of the discharged waste water at MHW initially increases expectedly due to the ebbing tide, and under the wind conditions considered.

For the Airport pump station the rate of increase in the spatial extent reduces as MLW is approached at approximately 6 hours after the initial release. At MLW initially the dilution rate increase as the waste water disperses over the exposed intertidal flats and associated intertidal channels. At the 4 hour mark the flooding tide effectively confines the discharged waste water to the immediate vicinity of the discharge point, and the spatial extent of the dilution field decreases. At 6 hours after MLW the momentum of the discharged waste water overcomes the tidal forcing and the plume of waste water extends away from the discharge point.

For the Songer pump station, the spatial extent reduces as MLW is approached at approximately 6 hours after the initial release. The discharge of wastewater under no-wind conditions from Songer pump station at MHW results in very limited plume extents due to the relatively shallow intertidal flats within the area and the ponding of the discharge. The spatial distribution of the discharged waste water at MLW is very limited due to the relatively shallow intertidal flats within the area and the ponding of the discharge. At 6 hours after MLW the momentum of the discharged waste water overcomes the tidal forcing and the plume of waste water extends away from the discharge point.

For the Saxton pump station, the initial spatial distribution of the discharged waste water at MLW increase as the waste water disperses over the exposed intertidal flats and associated intertidal channels. At the 4 and 6 hour mark after the beginning of the discharge the dilution plume is relatively diffuse for both wind events modelled, with similar spatial extents, presumably due to the relatively low wind speeds. In contrast, the plume associated with the no-wind event is confined to the vicinity of the discharge point due to the momentum balance between the flooding tide and the discharge rate.

For the Wakatu pump station, the spatial extent at 4 and 6 hours post the start of the discharging process is similar, consistent with the discharge of waste water over intertidal flats and channels. The spatial distribution of the discharged waste water at MLW is very limited due to the relatively shallow intertidal flats within the area and the ponding of the discharge. At 6 hours after MLW the momentum of the discharged waste water beings to overcome the tidal forcing and the plume of waste water extends slightly further away from the discharge point.

Files containing the temporally and spatially variable dilution fields for each of the pump stations have been supplied to client.

5. REFERENCES

Andrejev, O., K. Myrberg, and P.A. Lundberg. 2004. “Age and Renewal Time of Water Masses in a Semi-Enclosed Basin – Application to the Gulf of Finland.” *Tellus* 56 (5): 548–58.

Deleersnijder, E., J.-M. Campin, and E.J.M. Delhez. 2001. “The Concept of Age in Marine Modelling. I. Theory and Preliminary Model Results.” *Journal of Marine Systems* 25 (3–4): 229–67. doi:10.1016/S0924-7963(01)00026-4.

Egbert, G. D., and S. Y. Erofeeva. 2002. “Efficient Inverse Modeling of Barotropic Ocean Tides.” *Journal of Atmospheric and Oceanic Technology* 19 (2): 183–204.

Hall, T.M., and T.W.N. Haine. 2002. “On Ocean Transport Diagnostics: The Idealized Age Tracer and the Age Spectrum.” *Journal of Physical Oceanography* 32: 1987–91. doi:http://dx.doi.org/10.1175/1520-0485(2002)032<1987:OOTDTI>2.0.CO;2.

Kantha, L. H., and C. A. Clayson. 1994. “An Improved Mixed Layer Model for Geophysical Applications.” *Journal of Geophysical Research* 99 (C12): 25235–66.

Meier, H.E.M., and A. Höglund. 2013. “Studying the Baltic Sea Circulation with Eulerian Tracers.” In *Preventive Methods for Coastal Protection*, 101–29. Springer International Publishing.

Mellor, George L. 1998. *Users Guide for a Three Dimensional, Primitive Equation, Numerical Ocean Model*. Program in Atmospheric and Oceanic Sciences, Princeton University Princeton, NJ 08544-0710. http://jes.apl.washington.edu/modsims_two/usersguide0604.pdf.

MetOcean Solutions Ltd. 2017. “Bell Island Discharge and Dilution Modelling.” P0332.

Zhang, W.G., J.L. Wilkin, and O.M.E. Schofield. 2010. “Simulation of Water Age and Residence Time in New York Bight.” *Journal of Physical Oceanography* 40: 965–82. doi:http://dx.doi.org/10.1175/2009JPO4249.1.

Zhang, Y. L., and A. M. Baptista. 2008. “A Semi-Implicit Eulerian-Lagrangian Finite Element Model for Cross-Scale Ocean Circulation.” *Ocean Modelling* 21: 71–96.